The electronic structure of liquid alkali metals: calculation of photoemission spectra

1990 J. Phys.: Condens. Matter 2 5065

(http://iopscience.iop.org/0953-8984/2/22/025)

J. Phys.: Condens. Matter **2** (1990) 5065–5076. Printed in the UK

The electronic structure of liquid alkali metals: calculation of photoemission spectra

W Jank and J Hafner

Institut für Theoretische Physik, Technische Universität Wien, Wiedner Hauptstrasse 8–10, A-1040 Wien, Austria

Received 19 February 1990

Abstract. We present a first-principles calculation of the atomic structure (pair correlation function, static structure factor), the electronic structure (total and partial densities of states), and of the photoemission intensities of liquid Li and Na. We find that in liquid Li the electronic density of states shows a strong structure-induced 'Brillouin-kink' which leads to a pronounced narrowing of the width of the occupied band compared to the prediction of the free electron model. The DOS of liquid Na on the other hand is close to the free electon parabola. The origin of the difference is in the strong p component in the electron–ion potential in Li, but not in Na. The observed deviation of the photoemission spectrum of Na from a free electron form is explained in terms of the partial photoionisation cross-sections. A detailed comparison with experiment shows that the accuracy of the theoretical predictions is limited only by the local density approximation for the many-electron interactions.

1. Introduction

The electronic structure of the alkali metals is generally considered to be very close to the predictions of the free electron model. For sodium this is confirmed by the calculated spectra [1] and by photoemission studies [2] on polycrystalline samples, whereas a somewhat reduced bandwidth is suggested by photoemission investigations on single crystalline Na [3, 4]. For lithium, self-consistent band structure calculations predict rather substantial deviations from the free electron model, i.e. a reduced bandwidth and an increased density of states at the Fermi level [1].

For the liquid alkali metals the first reliable photoemission data have been published only very recently [5]. In complete analogy to the crystalline case it is found that the bandwidth of liquid Na is close to the free electron prediction, whereas a substantial reduction of the bandwidth is predicted for liquid Li. In addition the shape of the valence band is rather triangular (especially for Na), and hence not in immediate agreement with the free electron model. Numerical calculations of the electronic DOS have been performed using perturbation theory and using different Green function techniques [6, 7]. It is now generally accepted that perturbation theory is not sufficiently accurate for a determination of the electronic DOS: the imaginary part of the electronic self-energy which is of basic importance for the description of the broadening of the electronic states is neglected and hence perturbation theory leads to vastly exaggerated predictions of the deviations from the free electron model [8]. On the other hand, Green function calculations predict only minor deviations of the DOS from the free electron parabola,

0953-8984/90/225065 + 12 $03.50

for the alkali [9, 10] as well as for the polyvalent liquid metals [11]. Recent photoemission studies [12, 13] of the polyvalent liquid metals have demonstrated that strong deviations from a free electron DOS exist in many metals. Hence it is clear that the predictions of the various Green function approaches to the electronic DOS of the liquid metals must be considered with some scepticism.

Very recently we have presented a novel supercell approach to the electronic structure of liquid and amorphous materials [14–17]. A realistic model for the atomic arrangement in the melt or in the glass is generated via molecular dynamics simulation (a typical model contains between 50 and 70 atoms in a periodically repeated 'supercell'). Keeping the atomic coordinates fixed, any standard band structure technique can be used to calculate the electronic density of states. We have shown that both minimum basis-set methods such as the linear-muffin-tin-orbital method (LMTO) [14, 18, 19] and plane-wave basis methods such as dynamical simulated annealing (DSA) [17, 20] can be used quite efficiently for such large supercells. For the polyvalent liquid elements we have been able to predict densities of states and photoemission intensities in excellent agreement with experiment [15–17]. Furthermore, these results allow us to explore the correlations in the characteristic trends in the atomic and the electronic structure of liquid metals [16].

In this paper we apply these methods to an *ab initio* calculation of the atomic and electronic structure of liquid Li and Na: the atomic structure is calculated using molecular dynamics based on interatomic forces derived from optimised first-principles pseudopotentials. The electronic densities of states and the photoemission intensities are determined via the LMTO supercell method. Very good agreement with the neutron diffraction data for the static structure factor and with the measured photoelectron spectra is achieved. We find that the observed differences in the electronic DOS of liquid Li and Na arise from a 'Brillouin-kink' occurring roughly at the energy (in atomic units) $(Q_p/2)^2$ corresponding to a momentum transfer at which the static structure factor has its main maximum. This 'Brillouin-kink' is very weak in liquid Na, but quite pronounced in liquid Li. The triangular shape of the spectrum observed for liquid Na is shown to arise from a large photoionisation cross-section for p states.

2. Atomic structure

In the following we describe the calculation of the atomic structure of liquid Li and Na using pseudopotential-derived interatomic forces and molecular dynamics.

2.1. Interatomic forces

The calculation of the effective interatomic potential using second-order pseudopotential perturbation theory is a standard procedure [21, 22], one only has to specify the choice of a pseudopotential and of the local field corrections to the dielectric function in the random phase approximation. For the local field corrections we used the Vashishta–Singwi [23] form which satisfies the compressibility sum rule for the electron gas. The pseudopotentials of Li and Na are expected to be quite different: as Li has only s electrons in the core, the p component of the conduction band states feels the full electron–ion potential, whereas for Na both the s and p components are expected to be

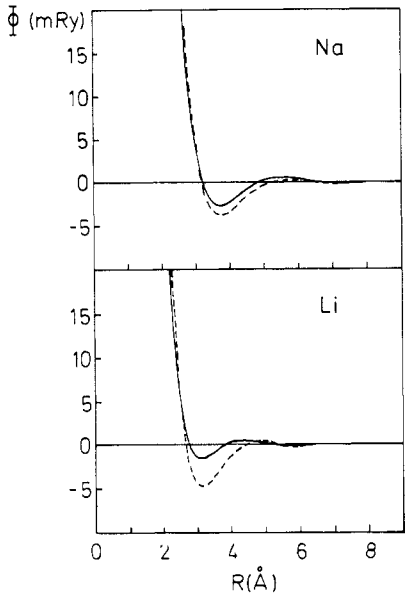

Figure 1. Effective interatomic pairpotential $\Phi(R)$ for liquid Na and Li. Full curve: calculated using a local empty-core pseudopotential; broken curve: calculated using a non-local optimised first-principles pseudopotential (see text). Atomic volume $\Omega = 41.32$ Å^3 for Na and $\Omega = 22.52$ Å^3 for Li.

weak. Hence the pseudopotential of Li should be stronger and considerably more non-local than the pseudopotential of Na. This difference in the potential is usually thought to account for the observed differences in the physical properties.

To study this point in detail we used two different sets of pseudopotentials: (i) a non-local optimised first-principles pseudopotential based on an orthogonalised plane-wave expansion of the conduction band states and a local density approximation for exchange and correlation (for details in the construction of the potential and for applications for lattice dynamical properties of the solid, liquid structure, etc, we refer to our earlier work [22, 24]); and (ii) a local empty-core pseudopotential [25] with the core radius R_c fitted to the zero-pressure condition at $T = 0$ K (Li: $R_c = 0.69$ Å, Na: $R_c = 0.94$ Å).

The interatomic potentials derived from both types of pseudopotentials are shown in figure 1. The potentials are almost identical in the repulsive part, the differences are in a somewhat deeper main minimum and a stronger damping of the Friedel oscillations in the pair interactions derived from the non-local pseudopotential.

2.2. Molecular dynamics simulation

The atomic structure of the liquid has been calculated by using a micro-canonical molecular dynamics simulation. The MD routine is based on a fifth-order predictor–corrector algorithm of the Newtonian equations of motion and an efficient network cube algorithm for nearest-neighbour book keeping. Details are given elsewhere [26, 27].

For each element we have performed two sets of MD simulations: one on a large ensemble of 1000 atoms/cell for the determination of accurate pair correlation functions and static structure factors, and a second for a small ensemble of 64 atoms/cell to generate the atomic coordinates for the electronic structure calculation using the super-cell method. For the large ensembles the pair potential was cut at a distance of $R_{cut} = 9.0$ Å for Na and $R_{cut} = 8.9$ Å for Li, close to a node in the potential. For the small

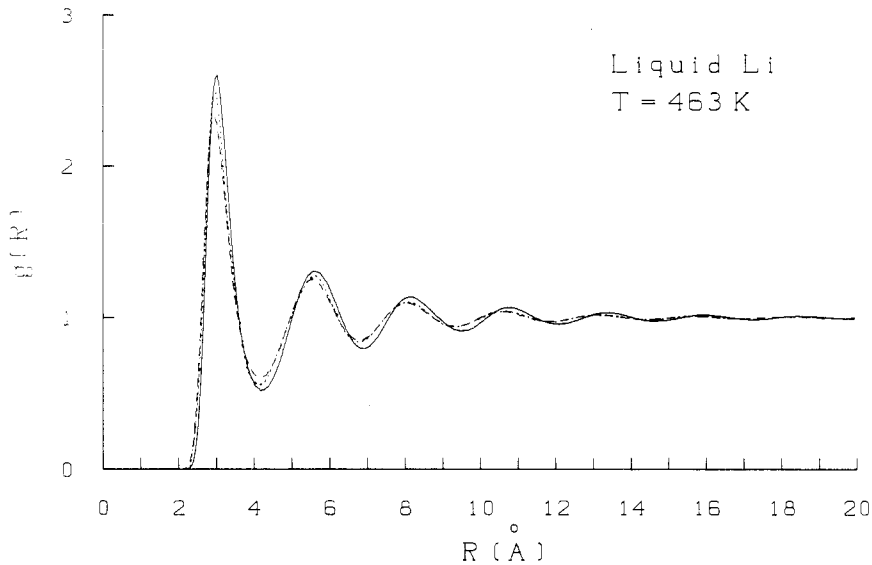

Figure 2. Pair correlation function $g(R)$ for liquid Li at $T = 463$ K. Full curve: calculated using the optimised first-principles pseudopotential; broken curve: calculated using the local empty-core pseudopotential; dotted curve: x-ray diffraction data (after Waseda [28]).

ensemble the potential was cut at the largest distance compatible with the minimum image convention (i.e. 50 per cent of the edge of the MD cell, $R_{cut} = 6.9$ Å for Na and $R_{cut} = 5.6$ Å for Li). The time step was set to $\Delta t = 1 \times 10^{-15}$ s for Li and $\Delta t = 2 \times 10^{-15}$ s for Na. Typical sampling runs extended over 5000 to 7000 time steps, up to 500 independent configurations being used for the calculation of a pair correlation function.

2.3. Pair correlation function and static structure factor

The pair correlation function $g(R)$ of liquid Li is shown in figure 2. As expected from the interatomic potential, the $g(R)$ calculated using the non-local pseudopotential differs from that calculated using the empty-core model by a somewhat larger amplitude of the oscillations and by a small phase shift. A similar difference is found in the static structure factor $S(q)$. A comparison with the experimental data at $T = 463$ K seems to indicate a slightly better agreement with the local pseudopotential calculation (figure 3(a)). However, the very accurate neutron scattering data of Olbrich *et al* [29] at $T = 593$ K are in nearly perfect agreement with the calculation using the non-local pseudopotential (figure 3(b)). For liquid Na the results obtained using the non-local and local pseudopotentials show hardly any difference, both results agree very well with the experimental data (figure 4).

In summary we conclude that the small differences in the structure functions derived from different pair potentials confirm the view that the liquid structure of the alkali metals is determined mainly by the repulsive part of the pair interaction [22] and that the theoretical results agree with experiment almost within the experimental uncertainty.

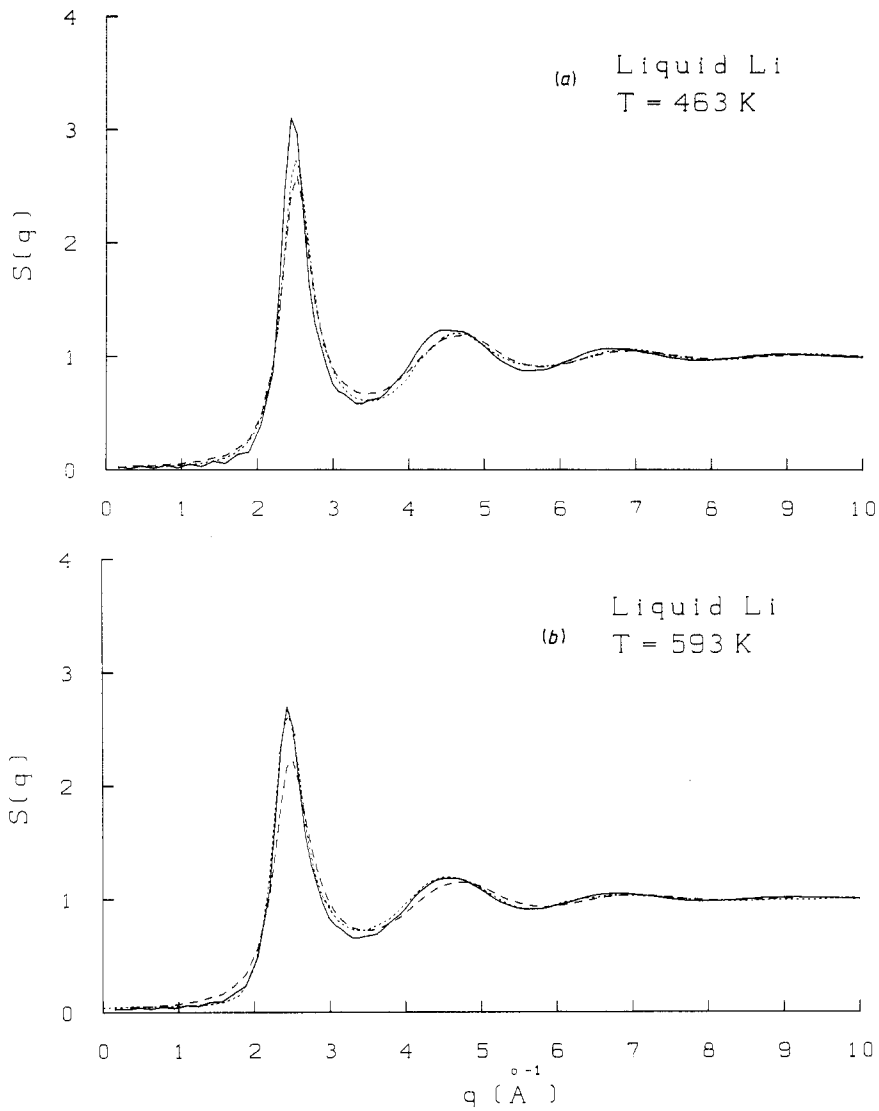

Figure 3. (*a*) Static structure factor $S(q)$ for liquid Li at $T = 463$ K. The full and broken curves represent the result of the MD simulations based on the non-local and local pseudopotentials respectively; the dotted curve gives the experimental results of Waseda [28]. (*b*) Static structure factor $S(q)$ for liquid Li at $T = 593$ K. For key, see figure 3(*a*). The experimental results are those of Olbrich *et al* [29].

3. Electronic structure

In the present work we have used the linearised-muffin-tin-orbital version of the supercell approach [14–16]. Our earlier work has shown that the dynamically simulated annealing approach based on local pseudopotentials is computationally more efficient and offers in addition the advantage that the atomic and electronic structures are consistent on a linear response level [17]. However, at the present stage the approach is

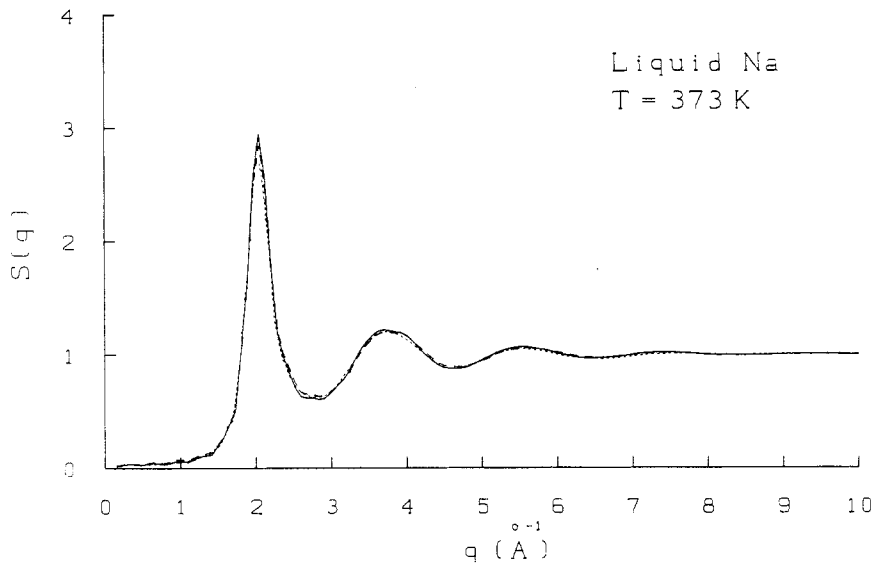

Figure 4. Static structure factor for liquid Na at $T = 373$ K. For key, see figure 3(*a*). The experimental results are those of Waseda [28].

limited to local and semi-local pseudopotentials but this might be problematic for Li. The advantage of the LMTO approach is that it yields the angular momentum decomposed densities of states, and that this information can be used to calculate the partial photoemission cross-sections as a function of the electron and photon energies.

3.1. LMTO-supercell calculations

The LMTO-supercell technique is well documented in our earlier work, so we can restrict ourselves to a few technical remarks:

(i) We used the scalar-relativistic version of the LMTO method in the atomic sphere approximation (ASA) [18, 19]. Exchange and correlation effects are described within the local density functional parametrisation of von Barth *et al* [30].

(ii) The electronic DOS is calculated by a Gaussian broadening of the discrete energy levels of the atoms in the supercell. As our results on the polyvalent liquid metals have shown, the DOS cannot be derived with sufficient accuracy from the eigenvalues calculated from a single $\boldsymbol{k}$ point. We used a mesh of four points in the irreducible part of the Brillouin zone of the supercell, the width of the Gaussian is set to $\sigma = 0.15$ eV.

(iii) In principle the calculation of the DOS of a liquid should be based on an average over independent configurations. However, it turns out that for 64-atom configurations with a pair correlation function close to the ensemble average of a 1000-atom model (figure 5), there are only minimal fluctuations in the electronic DOS. Hence it is in general sufficient to calculate the DOS for a very small number of atomic configurations.

We have also calculated the electronic DOS for the body centred cubic structures of Li and Na (atomic volume $\Omega_{Li} = 21.47$ Å^3, $\Omega_{Na} = 37.72$ Å^3). In this case the Brillouin zone integrations for the DOS have been performed using the linear tetrahedron method [31, 32].

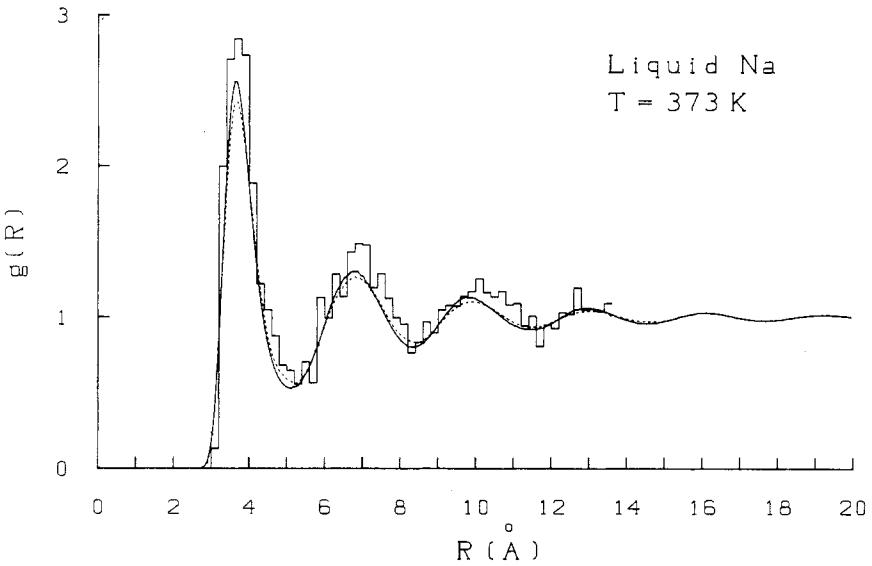

Figure 5. Pair correlation function $g(R)$ for liquid Na at $T = 373$ K calculated for a 1000-atom ensemble (full curve: configuration average over 480 independent configurations) and for a single 64-atom supercell (histogram). The dotted curve shows the diffraction data of Waseda [28].

3.2. Electronic density of states

The electronic DOS of liquid and solid Li is shown in figure 6. For both crystalline BCC and liquid Li the calculations predict strong deviations from a free electron parabola. In the crystalline case it is well known that the DOS minimum at an energy of ~2.6 eV above the Fermi energy and the maximum close to E_F originate from a large gap at the N point whose width is directly proportional to the $Q(110)$ matrix element of the pseudopotential (for BCC Li we have $|Q(110)| = 2.54$ Å^{-1}, hence the energy $(|Q(110)|/2)^2 = 6.13$ eV is just $\simeq 2.6$ eV larger than the Fermi energy in BCC Li). The strong increase of the DOS at the Fermi level by nearly a factor of 1.5 compared to the free electron value leads to the reduction of the bandwidth from $W_{FE} = 4.72$ eV to $W = 3.45$ eV.

The origin of the deviation from the free electron model in liquid Li is essentially the same: the sharp first peak in the structure factor at $|Q_p| = 2.5$ Å^{-1} acts as a smeared-out reciprocal lattice vector and induces a DOS minimum (a 'pseudogap') at an energy of $|Q_p/2|^2 = 5.95$ eV above the bottom of the band. States with $|q| \leq Q_p/2$ may be considered to be in the first 'pseudo-Brillouin zone', and the pseudogap is the equivalent of the Brillouin-kink in the DOS of crystalline materials. Due to the finite width of the peak in $S(q)$, the structures in the DOS are also broadened, but the increase of the DOS at E_F and the bandwidth of $W = 3.5$ eV are essentially the same as for crystalline Li. In our estimate of the bandwidth for the liquid metal we ignore the small tail which is an artefact due to the Gaussian broadening. From their photoemission data Indlekofer *et al* [5] deduce a bandwidth of $W = 3.2 \pm 0.2$ eV.

The partial DOS of the occupied part of the band can be described as essentially semi-elliptic for s states and more or less triangular for p and d states. In the empty part of the conduction band we find that the structure induced features are strongest in the p component of the DOS, as expected for the non-local potential of the Li core.

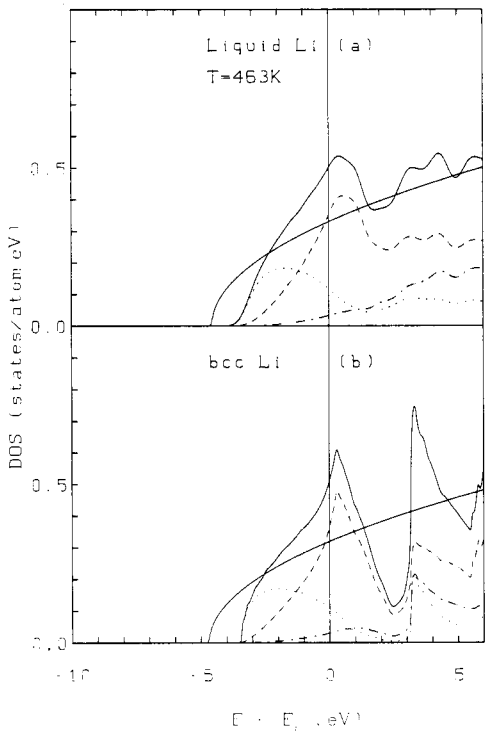

Figure 6. Electronic density of states in liquid Li at $T = 463$ K (*a*) and in BCC Li (*b*). Full curve: total DOS; dotted curve: partial DOS of s states; broken curve: p states; chain curve: d states. The free electron parabola has been drawn for comparison.

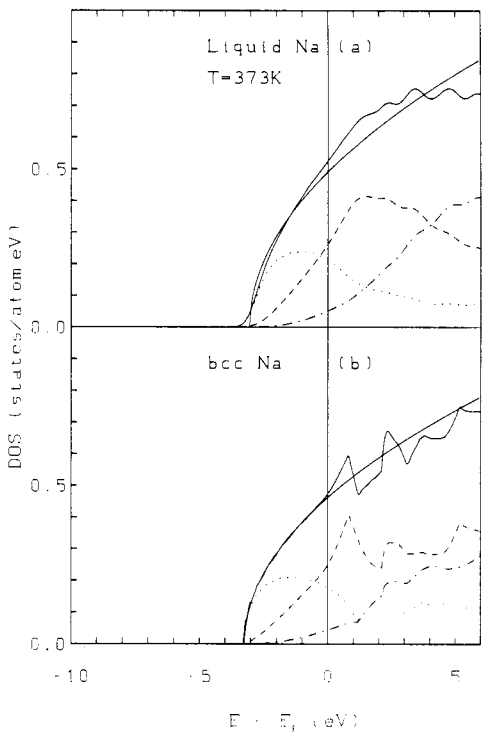

Figure 7. Electronic density of states in liquid Na at $T = 373$ K (*a*), and in BCC Na (*b*). For key, see figure 6.

In the electronic DOS of BCC and liquid Na we find essentially the same structure induced features, but they are now much weaker than in Li—as expected. For both the solid and liquid phases the calculated bandwidth is almost identical to the free electron prediction ($W_{FE} = 3.24$ eV for BCC Na, $W_{FE} = 3.04$ eV for l-Na). Again this is just on the upper edge of the estimate of $W = 2.8 \pm 0.2$ eV deduced from the photoemission data on l-Na and somewhat larger than the value of $W = 2.65 \pm 0.05$ eV deduced from the angular resolved photoemission data on single crystalline BCC Na.

3.3. Photoemission intensities

A quantitative analysis of the shape of the photoelectron spectra requires a calculation of the photoemission intensities. If all effects associated with the transport of the photoelectron to the surface and its escape from the surface are neglected, then the energy distribution of the photoemitted electrons is given according to the golden rule by [33]

$$I(E, \hbar\omega) \sim \sum_{i,f} \int d\boldsymbol{k} |\langle f|\boldsymbol{A}\cdot\boldsymbol{p}|i\rangle|^2 \delta(E_f(\boldsymbol{k}_f) - E_i(\boldsymbol{k}_i) - \hbar\omega)\delta(E - E_f(\boldsymbol{k}_f)) \qquad (1)$$

where i and f denote initial and final states respectively. The following approximations

allow the calculation of $I(E, \hbar\omega)$ in terms of the self-consistent one-electron potential and the partial densities of state $n_l(E)$ [34–36]:

(i) dipole approximation to the photon field characterised by the vector potential $\boldsymbol{A}$;
(ii) complete neglect of wavenumber conservation;
(iii) single scatterer—final state approximation;
(iv) independent averages over all $\boldsymbol{k}_f$ directions and photon directions and polarisations.

The resulting expression for the angle integrated photoelectron intensity is given by

$$I(E, \hbar\omega) \propto \frac{1}{\omega^2} \sum_l n_l(E)\sigma_l(E, \hbar\omega) \tag{2}$$

where the $\sigma_l(E, \hbar\omega)$ are the partial photoionisation cross-sections [36]:

$$\sigma_l(E, \hbar\omega) = \sum_{l'=l\pm1} (2l'+1)\begin{pmatrix} l' & 1 & l \\ 0 & 0 & 0 \end{pmatrix} \left| \int_0^S R_{l'}(E+\hbar\omega, r) \frac{\mathrm{d}V(r)}{\mathrm{d}r} R_l(E, r) r^2 \, \mathrm{d}r \right|^2 . \tag{3}$$

Here the R_l are the regular solutions of the radial Schrödinger equation and $V(r)$ is the muffin-tin potential. The integration is over the atomic sphere only.

The crucial point is approximation (ii). For the crystal it has been shown that phonon broadening relaxes the condition of wavevector conservations for higher excitation energies, $\hbar\omega \geq 200$ eV. Hence in this case the result (2, 3) can be used for the calculation of x-ray photoemission spectra (XPS) only. In the liquid where there is no translational invariance, the wavevector is not a conserved quantity, hence the result can be used also for the lower excitation energies of ultraviolet photoemission spectroscopy (UPS).

The calculated photoemission intensities and photoionisation cross-sections for liquid Li and Na are given in figures 8 and 9 for a series of photonenergies in the UPS and XPS range. The calculated DOS has been multiplied by a Fermi function, for the XPS spectrum the calculated intensity has been additionally Gaussian broadened ($\sigma =$ 0.5 eV). For liquid Li we find a very good agreement with the experiment: at all excitation energies the spectrum is dominated by the s states and this leads to a rounded form of the spectrum. At lower photon energies ($\hbar\omega = 11.8$ eV, 16.8 eV) the p contribution is somewhat increased and this results in a slightly more triangular form of the spectrum. The broad feature near $E_B = 4.2$ eV in the ArI ($\hbar\omega = 11.8$ eV) spectrum arises from a surface plasmon [5].

In liquid Na the p electron photoionisation cross-section is now of the same magnitude as the s electron cross-section. This, together with the increase of both cross-sections for lower binding energy explains very nicely the triangular form of the photoemission spectrum.

4. Conclusions

We have presented an *ab initio* calculation of the atomic and electronic structure, and of the photoemission spectrum of liquid Li and Na.

For liquid Li we find a strong structure induced minimum in the electronic DOS at an energy of approximately $|\boldsymbol{Q}_p/2|^2$ above the bottom of the band (where $\boldsymbol{Q}_p$ is the wavevector corresponding to the main peak in the static structure factor) and a strongly

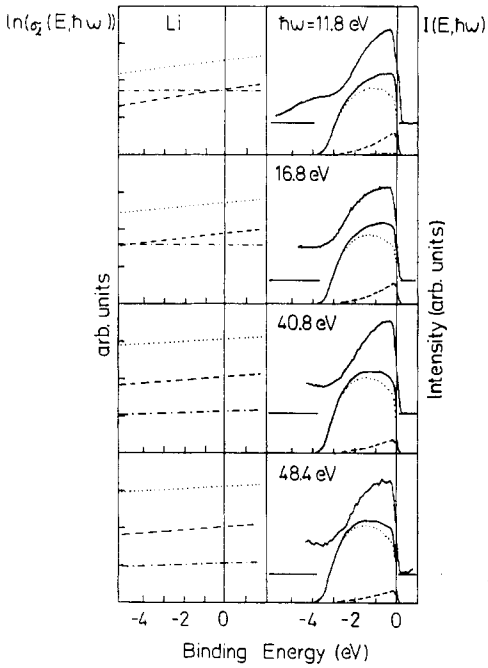

Figure 8. Calculated and measured photoemission intensities $I(E, \hbar\omega)$ and the calculated partial photoionisation cross-section $\sigma_l(E, \hbar\omega)$ for liquid Li at different energies of the exciting photon. Full curve: total calculated and experimental photoemission intensity (after [5]); dotted curve: s-; broken curve: p-; and chain curve: d-electron contributions. For the sake of clarity the zero of the experimental intensity has been shifted.

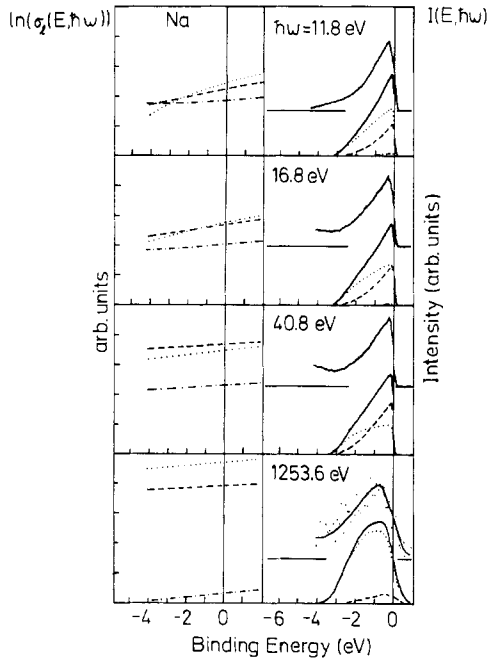

Figure 9. Calculated and measured photoemission intensities $I(E, \hbar\omega)$ and the calculated partial photoionisation cross-section $\sigma_l(E, \hbar\omega)$ for liquid Na at different energies of the exciting photon; compare with figure 8. The full curve in the experimental XPS spectrum represents a guide to the eye.

enhanced DOS at lower energies, resulting in a bandwidth which is strongly reduced compared to the free electron value.

For liquid Na only very weak structure induced features are found in the DOS, which is essentially like a free electron.

The different behaviour of Li and Na is clearly due to the strong p component of the electron–ion potential of Li.

The theoretical predictions of both the atomic and electronic structures are found to be in very good agreement with experiment. For the atomic structure, theory and experiment agree essentialy to within the accuracy of the experimental data. For the electronic structure, the most important limitation to the accuracy of the theoretical prediction arises from the local density approximation. For crystalline Na it has been shown that a wavevector dependent self-energy correction accounts for the difference between the measured quasiparticle band structure and the prediction of local density functional theory. In the liquid any $\boldsymbol{k}$ dependent features are smeared out and this would seem to account for the fact that the gap between the photoemission data and the self-consistent electronic structure calculations is smaller for the liquid than for the crystalline

metal. The triangular shape of the measured photoemission spectrum of liquid Na has been interpreted as representing a deviation from a free electron behaviour. Our results show that this is not correct. The DOS is of a perfect free electron form, the observed shape of the spectrum results from the difference in the s and p photoionisation cross-sections, and from their variation with the binding energy.

Acknowledgments

We thank Professor P Weinberger and Dr J Redinger for the computer program used to calculate the photoionisation cross-sections. The numerical calculations were performed on an IBM 3090-400 VF at the Computer Centre of the University of Vienna, supported by the IBM European Academic Supercomputer Initiative (EASI). Financial support from the Fonds zur Förderung der wissenschaftlichen Forschung (Austrian Science Foundation) under project No 7192 is gratefully acknowledged.

References

[1] Moruzzi V L, Janak J F and Williams A R 1978 *Calculated Electronic Properties of Metals* (New York: Pergamon)
[2] Höchst H, Steiner P and Hüfner S 1978 *Z. Phys.* B **30** 145
[3] Jensen E and Plummer E W 1985 *Phys. Rev. Lett.* **55** 1912
[4] Lyo I W and Plummer E W 1988 *Phys. Rev. Lett.* **60** 1558
[5] Indlekofer G and Oelhafen P 1990 *Proc. 7th Int. Conf. on Liquid and Amorphous Metals (LAM7)*; *J. Non-Cryst. Solids* **117 + 118** 340
[6] Shimoji M 1977 *Liquid Metals* (New York: Academic) p 133
[7] Cusack N E 1987 *The Physics of Structurally Disordered Matter* (Bristol: Hilger) p 175
[8] Ballentine L E 1975 *Adv. Chem. Phys.* **31** 263
[9] Itami T and Shimoji M 1972 *Phil. Mag.* **25** 229
[10] Kuroha M and Suzuki K 1974 *Phys. Lett.* **47A** 329
[11] Van Oosten A B and Geerstma W 1985 *Physica* B **133** 55
[12] Oelhafen P, Indlekofer G and Güntherodt H J 1988 *Z. Phys. Chem.* **157** 483
[13] Indlekofer G, Oelhafen P, Lapka R and Güntherodt H J 1988 *Z. Phys. Chem.* **157** 465
[14] Hafner J and Jaswal S S 1988 *Phys. Rev.* B **38** 7320
[15] Jank W and Hafner J 1988 *Europhys. Lett.* **7** 623
[16] Jank W and Hafner J 1990 *Phys. Rev.* B **41** 1497
[17] Hafner J and Payne M C 1990 *J. Phys.: Condens. Matter* **2** 221
[18] Andersen O K, Jepsen O and Glötzel D 1985 *Highlights of Condensed Matter Theory* ed F Bassani, F Fumi and M P Tosi (Amsterdam: North-Holland)
[19] Skriver H L 1984 *The LMTO Method (Springer Series in Solid State Sciences 41)* (Berlin: Springer)
[20] Car R and Parrinello M 1985 *Phys. Rev. Lett.* **55** 2471
[21] Heine V and Weaire D 1970 *Solid State Physics* vol 24 (New York: Academic) p 247
[22] Hafner J 1987 *From Hamiltonians to Phase Diagrams (Springer Series in Solid State Sciences 70)* (Berlin: Springer)
[23] Vashishta P and Singwi K S 1972 *Phys. Rev.* B **6** 875
[24] Hafner J 1976 *Z. Phys.* B **24** 41
[25] Ashcroft N W 1966 *Phys. Lett.* **23** 48
[26] Arnold A, Mauser N and Hafner J 1989 *J. Phys.: Condens. Matter* **1** 965
[27] Arnold A and Mauser N 1990 *Comp. Phys. Commun.* at press
[28] Waseda Y 1981 *The Structure of Non-Crystalline Materials—Liquids and Amorphous Solids* (New York: McGraw-Hill) p 253 ff
[29] Olbrich H, Ruppersberg H and Steeb S 1983 *Z. Naturf.* a **38** 1328
[30] von Barth U, Hedin L and Janak J F 1975 *Phys. Rev.* B **12** 1257
[31] Jepsen O and Andersen O K 1971 *Solid State Commun.* **9** 1763

[32] Lehmann G and Taut M 1972 *Phys. Status Solidi* b **54** 469
[33] Cardona M and Ley L 1979 *Photoemission in Solids I (Springer Topics in Applied Physics 26)* (Berlin: Springer) p 1
[34] Jarlborg T and Nilsson P O 1979 *J. Phys. C: Solid State Phys.* **12** 265
[35] Winter H, Durham P J and Stocks G M 1984 *J. Phys. F: Met. Phys.* **14** 1047
[36] Redinger J, Marksteiner P and Weinberger P 1986 *Z. Phys.* B **63** 321